

Off-shell ω production in proton-proton collisions near threshold

C. Fuchs^a, M.I. Krivoruchenko^{a,b}, H.L. Yadav^{a,c}, Amand Faessler^a, B.V. Martemyanov^{a,b}, K. Shekhter^a

^a *Institut für Theoretische Physik der Universität Tübingen, Auf der Morgenstelle 14, D-72076 Tübingen, Germany*

^b *Institute for Theoretical and Experimental Physics, B. Chermushkinskaya 25, 117259 Moscow, Russia*

^c *Physics Department, Rajasthan University, Jaipur-302004, India*

The ω production in nucleon-nucleon collisions is described through the decay of intermediate nuclear resonances. Close to threshold the $pp \rightarrow pp\omega$ cross section is dominated by the off-shell production of ω mesons with masses far below the physical ω mass of 782 MeV. A crucial role plays thereby the $N^*(1535)$ resonance. Due to a strong $N\omega$ decay mode this resonance leads to off-shell contributions which are in the vicinity of the threshold about one order of magnitude larger than the experimentally measurable contribution from only the ω peak. After a subtraction of the theoretical "background" from off-shell ω production the available data are accurately reproduced over the entire energy range from very close to threshold up to several GeV above threshold. The scenario of a weaker $N^*(1535) \rightarrow N\omega$ decay mode which is still consistent with electro- and photo-production data is discussed as well. In the latter case the off-shell contributions to the $pp \rightarrow pp\omega$ cross section are substantially reduced but the description of the experimental cross section is poor above threshold.

13.60.Le, 14.20.Gk, 25.40-h

I. INTRODUCTION

The studies of vector meson production in nucleon-nucleon collisions are motivated by several facts. Firstly, the short range part of the nucleon-nucleon (NN) interaction is dominated by the iso-scalar ω meson exchange [1] and thus information from inelastic NN collisions can contribute to a better understanding of the nuclear forces. In a dense hadronic environment which exists in the interior of neutron stars or is transiently created in energetic heavy ion reactions one expects significant changes of the quark condensates which should reflect in mass shifts of the vector mesons [2], suggested also by QCD sum rules [3]. In a hadronic picture the coupling to many-body correlations modifies the in-medium masses and the spectral properties of the mesons [4,5]. To search for modifications of the in-medium properties of vector meson is the major issue of dilepton spectroscopy in energetic heavy ion collisions [6].

However, for the study of medium effects in heavy ion reactions the theoretical understanding of vector meson production in elementary processes is a prerequisite. In the vicinity of the threshold only the ω production has been studied experimentally. This is due to the small ω width of 8.4 MeV which allows an identification of the narrow ω peak in missing mass spectra already close to

threshold. Data for the ω production in proton-proton ($pp \rightarrow pp\omega$) collisions at small excess energies were recently taken at SATURNE [7] and with the COSY-TOF spectrometer [8]. The excess energy ϵ is thereby defined as $\epsilon = \sqrt{s} - (2m_p + m_\omega)$ with \sqrt{s} being the proton-proton center-of-mass energy, m_p the proton mass and $m_\omega = 782$ MeV the physical ω mass at its pole value. The SATURNE experiment was performed very close to threshold ($\epsilon = 4 \div 30$ MeV) whereas the COSY-TOF Collaboration measured the ω production at $\epsilon = 92$ and 173 MeV. Both experiments served also to examine the validity of the Okubo-Zweig-Iizuka (OZI) selection rule [9]. Compared to the ω cross section, the ϕ meson which couples to the strangeness content of the nucleon should be strongly suppressed by the OZI rule which forbids disconnected quark line diagrams. According to only a small OZI violation a suppression factor of the ϕ over ω ratio at comparable excess energies of $\phi/\omega \sim 4 \cdot 10^{-3}$ has been predicted [10] while experimentally this ratio was found to be in pp reactions by about one order of magnitude larger [7,8,11] as expected.

Microscopic calculations for the ω production in nucleon-nucleon collisions are, however, rare. In ref. [12] the on-shell ω production was described through the couplings to nucleon currents and to meson exchange currents taking thereby the NN final-state interaction into account. The ω -meson was treated as an elementary field, thus off-shell effects in the ω production were missing from the beginning. Adjusting the relevant form factors, the experimental data [7] in the vicinity of the threshold were well reproduced.

In the present approach the vector meson production is described through a two-step mechanism via the excitation of nuclear resonances. This picture is motivated by the existence a variety of nucleon resonances which have large branchings to the $N\rho$ decay modes, such as $N^*(1520)\frac{3}{2}^-$, $N^*(1535)\frac{1}{2}^+$, and $N^*(1720)\frac{3}{2}^+$. The couplings with the ω -mesons are observed from the multi-channel πN partial wave analysis [28,14] and predicted by quark models [27]. A strong coupling of the $N\omega$ system to nuclear resonances has also been reported using an effective field theory coupled channel approach [16]. It is also a well established fact that within a hadronic picture the coupling to the nuclear resonances is a major source for the modification of the vector meson properties in a dense nuclear environment. E.g. in the medium the ρ acquires its major modifications by the coupling to the N^* -hole excitations, especially the $N^*(1520)N^{-1}$ [4,5].

The resonance model provides a unified description of a large variety of phenomena such as nucleon electro- and photoproduction, mesonic decays of nuclear resonances and vector meson production in elementary nucleon-nucleon reactions. The resonance decay modes to vector mesons can be fixed from electro-, photoproduction and mesonic decay data [5,17,18] and the resonance production cross sections from $NN \rightarrow NN\pi$ scattering data [19]. In this way there enter no new parameters in the description of the vector meson production in nucleon-nucleon reactions. The model is described in the next section. Close to threshold the behavior of the $pp \rightarrow pp\omega$ cross section turns thereby out to depend in a crucial way on the properties of the $N^*(1535)$ resonance. The analysis of [18] on which the present calculations are based predicts a large $N^*(1535)N\omega$ coupling which, as will be seen in the following, gives rise to large off-shell contributions in the $pp \rightarrow pp\omega$ cross section close the ω production threshold. To estimate the influence of the $N^*(1535)$ we consider also the case of a weaker $N^*(1535)N\omega$ coupling which is still compatible with the existing electro-, photoproduction and mesonic decay data for the $N^*(1535)$. When the $pp \rightarrow pp\omega$ cross section is compared to experimental data one has to keep in mind that experimentally only the distinct ω peak can be resolved in missing mass spectra. Off-shell contributions are attributed to the general experimental background. When a comparison to data is performed, in particular when off-shell contributions are large, this fact has to be taken into account and only the experimentally measurable part of the cross section should be considered. We apply such a procedure when the comparison to data is performed in Sec. III. The experimental data, in particular in the vicinity of the threshold, support the picture of a strong coupling of the $N^*(1535)$ to the $N\omega$ channel with the consequence of large off-shell contributions to the cross section.

II. RESONANCE MODEL

The vector meson production is described through a two-step mechanism via the excitation of nuclear resonances, i.e. $NN \rightarrow NR$, $R \rightarrow NV$, with $V = \rho, \omega$. The nucleon-nucleon cross section for the resonance production $NN \rightarrow NR$ have been determined by fitting the available data on pion, double-pion, η and ρ production $NN \rightarrow NNP, NNV$, and $NNPP$ reactions ($P = \pi, \eta, \dots$), within the two-step resonance model $NN \rightarrow NR$ with the subsequent decays of the resonances R 's [19]. Effects of the NN final-state interaction which are expected to be important near the threshold for all reactions are included into the phenomenological matrix elements \mathcal{M}_R 's for the resonance production. On the other hand, the present approach accounts also effectively for the final state interaction between one nucleon and the produced vector meson. To take the final-state interaction between the nucleon and the meson in specific

partial waves into account is equivalent to the inclusion of the nuclear resonances into the reaction dynamics which have the same quantum numbers as the corresponding partial waves (final-state interaction theorem).

In refs. [5,17,18], the Vector Meson Dominance (VMD) model was applied to determine the $RN\omega$ coupling strengths from radiative and mesonic decay data. In its monopole form, i.e. only including ground-state ρ and ω , the naive VMD is known to underestimate systematically the mesonic $R \rightarrow N\rho$ decays when a normalization to radioactive $R \rightarrow N\gamma$ branchings is performed [20]. The inclusion of higher ρ meson radial excitations in the VMD helps to resolve this problem [20,18] and provides the correct asymptotics of the $R \rightarrow N\gamma$ transition form factors given by the quark counting rules [21]. The extended (e)VMD model assumes that radial excitations $\rho(1450), \rho(1700), \dots$ interfere with the ground-state ρ -mesons in radiative processes. Already in the case of the nucleon form factors, radially excited vector mesons should be added in order to provide a dipole behavior for the Sachs form factors and describe the experimental data [22]. The details of calculations of the magnetic, electric, and Coulomb $R \rightarrow N\gamma$ transition form factors and the branching ratios of the nucleon resonances can be found in refs. [18,23]. The model parameters are fixed from photo- and electro-production data and using results of the multichannel partial-wave analysis of the πN scattering. Where experimental data are not available, predictions of the non-relativistic quark models are used. In [24] the same model was successfully applied to a systematic study of meson decays to dilepton pairs and in [20] to the description of dilepton production in pp reactions [25].

The $pp \rightarrow pp\omega$ cross section is then given as follows

$$\frac{d\sigma(s, M)^{pp \rightarrow pp\omega}}{dM^2} = \sum_R \int_{(m_p+M)^2}^{(\sqrt{s}-m_p)^2} d\mu^2 \frac{d\sigma(s, \mu)^{pp \rightarrow pR}}{d\mu^2} \frac{dB(\mu, M)^{R \rightarrow p\omega}}{dM^2} . \quad (1)$$

The cross sections for the resonance production are given by

$$d\sigma(s, \mu)^{pp \rightarrow pR} = \frac{|\mathcal{M}_R|^2}{16p_i \sqrt{s} \pi^2} \Phi_2(\sqrt{s}, \mu, m_p) dW_R(\mu) \quad (2)$$

with $\Phi_2(\sqrt{s}, \mu, m_p) = \pi p^*(\sqrt{s}, \mu, m_p)/\sqrt{s}$ being the two-body phase space, $p^*(\sqrt{s}, \mu, m_p)$ the final c.m. momentum, p_i the initial c.m. momentum, and μ and m_R the running and pole masses of the resonances, respectively. The mass distribution $dW_R(\mu)$ of the resonances is described by the usual Breit-Wigner formula:

$$dW_R(\mu) = \frac{1}{\pi} \frac{\mu \Gamma_R(\mu) d\mu^2}{(\mu^2 - m_R^2)^2 + (\mu \Gamma_R(\mu))^2} . \quad (3)$$

The sum in (1) runs over the nucleon resonances given in Table 1. This includes all well established (4*) resonances quoted by the PDG [26].

Nucleon resonances with spin $J > 1/2$ and arbitrary parity have three independent transition amplitudes, while spin-1/2 resonances have only two independent amplitudes. In terms of the magnetic, electric, and Coulomb couplings $g_M^{(\pm)}$, $g_E^{(\pm)}$, and $g_C^{(\pm)}$, the differential decay widths of nucleon resonances with spin $J = l + 1/2$ into an ω -meson with an off-shell mass M has the form [18]

$$d\Gamma_{N\omega}^R(\mu, M) = \frac{9}{64\pi} \frac{(l!)^2}{2^l(2l+1)!} \times \frac{m_{\pm}^2(m_{\mp}^2 - M^2)^{l+1/2}(m_{\pm}^2 - M^2)^{l-1/2}}{\mu^{2l+1}m^2} \left(\frac{l+1}{l} \left| g_{M/E}^{(\pm)} \right|^2 + (l+1)(l+2) \left| g_{E/M}^{(\pm)} \right|^2 + \frac{M^2}{\mu^2} \left| g_C^{(\pm)} \right|^2 \right) dW_{\omega}(M), \quad (4)$$

where μ refers to the resonance mass and m is the nucleon mass, $m_{\pm} = \mu \pm m$. The signs \pm refer to the natural parity ($1/2^-, 3/2^+, 5/2^-, \dots$) and abnormal parity ($1/2^+, 3/2^-, 5/2^+, \dots$). $g_{M/E}^{\pm}$ means g_M^+ or g_E^- . The above equation is valid for $l > 0$. For $l = 0$ ($J = 1/2$), one gets

$$d\Gamma_{N\omega}^R(\mu, M) = \frac{1}{32\pi\mu} (m_{\pm}^2 - M^2)^{3/2} (m_{\mp}^2 - M^2)^{1/2} \times \left(2 \left| g_{E/M}^{(\pm)} \right|^2 + \frac{M^2}{\mu^2} \left| g_C^{(\pm)} \right|^2 \right) dW_{\omega}(M). \quad (5)$$

The mass distribution $dW_{\omega}(M)$ of the ω is described by Eq. (3) with substitutions $R \rightarrow \omega$ and $\mu \rightarrow M$. Due to the subthreshold character of the ω production in decays of on-shell nucleon resonances, the M -dependence of the coupling constants $g_M^{(\pm)}$, $g_E^{(\pm)}$, and $g_C^{(\pm)}$ can be important. At $M = m_{\omega}$ these couplings are proportional to residues of the magnetic, electric, and Coulomb transition form factors at $M^2 = m_{\omega}^2$ and their values can be found in Table 1. We assume that the analogous coupling constants corresponding to the covariant form factors are not mass dependent. The M -dependence in $g_M^{(\pm)}$, $g_E^{(\pm)}$, and $g_C^{(\pm)}$ arises then due the M -dependent transformation from the covariant basis to the multi-pole basis according to

$$g_T^{(\pm)}(M^2) = \sum_{kT'} M_{Tk}(M^2) M_{kT'}^{-1}(m_{\omega}^2) g_{T'}^{(\pm)}(m_{\omega}^2), \quad (6)$$

with $T, T' = M, E, C$. The matrices $M_{kT}(M^2)$ which transform the multi-pole form factors to the covariant form factors can be found in ref. [18].

From the resonances which lie far below the ω peak the $N^*(1535)$ is the only one which has a large branching to the $N\omega$ channel. The strong $N^*(1535)N\omega$ coupling is obtained in ref. [18]. Since it will turn out that the considered cross section reacts very sensitive on this fact, in particular close to threshold, we consider also an alternative scenario with a weaker $N^*(1535)N\omega$ coupling. In the eVMD model the $N\rho$ and $N\omega$ decays are fixed simultaneously. However, in the case of the $N^*(1535)$

there were neither experimental data nor quark model predictions for the $N\omega$ channel available [18]. The available data in the $N\rho$ channel and the fact that quark models provide here partially contradictory results leave some freedom in the determination of the $N^*(1535)N\omega$ coupling strength. In Fig. 11 shown in the Appendix, we discuss two different fits to the electro- and photo-production data, the πN multichannel scattering, and quark model predictions in more detail. The essential distinction between these two procedures lies in the different normalizations to the ρ -meson decay amplitudes. Koniuk [27], Manley and Saleski [28], and the PDG [30] give close predictions for the $s_{1/2}$ wave and predict the same sign for the $d_{3/2}$ wave. The second set of amplitudes stems from quark model calculations by Capstick and Roberts [29]. Their values are noticeable smaller than those proposed by [27,28,30]. Both sets do not provide ω -meson amplitudes. To investigate the stability of our results, we introduced one point for the ω -meson $s_{1/2}$ wave around zero. The original solution [18], that uses the results of refs. [27,28,30] turns out to be rather stable and does not allow for a significant reduction of the $s_{1/2}$ wave amplitude. The second set allows the reduction of the amplitude by a factor of 6 to 8, however, by the price of a moderately higher χ^2 . A further going reduction of the amplitude is hardly possible. The deviation from the experiment for the Coulomb amplitude of the $p^*(1535)$ becomes then stronger and the quality of the fit for the transversal amplitude of the $p^*(1535)$ is also worse, but the ρ -meson amplitudes are reproduced better than for the first set of input parameters. Notice that the $d_{3/2}$ amplitude of the ω -meson was set equal to zero to ensure an unique eVMD solution to the fitted data. The value of $d_{3/2}$ does not affect significantly other observables.

In Table 1 the corresponding values for the $N\omega$ decay widths are given at the resonance pole masses. The branching of the $N^*(1440)$ at the resonance pole is small, since it lies deeply below the $N\omega$ threshold. However, the off-mass shell $N^*(1440)$'s with higher masses have noticeable ω decay widths. In Table 1, the contributions from different partial waves, including relative signs, are also shown. In the case of the $N^*(1535)$ the values for the two different fits resulting in a strong (s), respectively a weaker (w) coupling to the $N\omega$ channel are given. The corresponding matrix elements \mathcal{M}_R for the resonance production in pp collisions, Eq. (2), are taken from ref. [19].

The energy dependent total width $\Gamma_R^{[0]}(\mu)$ of the resonance is scaled according to the πN phase space and the Blatt-Weisskopf suppression factor. In a consistent treatment, the $N\rho$ and $N\omega$ decay channels have to be taken into account in the total width

$$\Gamma_R(\mu) = \Gamma_R^{[0]}(\mu) + \Gamma_{N\rho}^R(\mu) + \Gamma_{N\omega}^R(\mu) + \delta\Gamma_R \quad (7)$$

where $\delta\Gamma_R = -\Gamma_{N\rho}^R(m_R) - \Gamma_{N\omega}^R(m_R)$ ensures the normalization of the total width at the resonance pole mass m_R . Since the total width appears in the nominator and

squared in the denominator of the corresponding Breit-Wigner distribution (3) the partial widths are not simply added in a perturbative way but the coupled channel problem is more complicated. The appearance of new channels shifts generally strength from the pole to the tails of the distribution. However, the shape of the spectral function around the ω pole depends crucially on the magnitude of the partial decay width. In the case of a strong $N\omega$ coupling, the rapidly increasing partial width leads to a strong reduction at the ω threshold, an effective enhancement below the ω peak, and shifts strength further out. A weak coupling, on the other hand, leads to visible ω -peak in the resonance spectral function. The consequences of these two different scenarios will become more clear when the cross sections are considered in the next section.

In Fig. 1 we show the energy dependence of the $N^* \rightarrow N\omega$ widths versus the off-shell masses μ of the resonances with the ω spectral function of ref. [18]. We show two solutions for the $N^*(1535)$ resonance: The dot-dashed line refers to the original set of input parameters with strong coupling (s) while the solid line refers to the new set with weaker coupling (w).

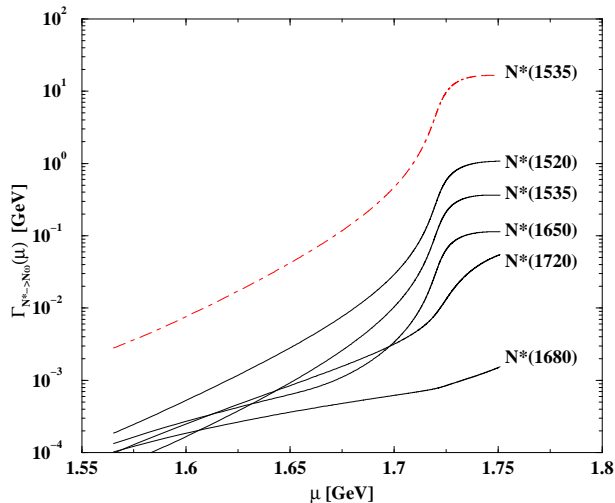


FIG. 1. Energy dependence of the $N^* \rightarrow N\omega$ widths versus the off-shell masses μ of the resonances. For the $N^*(1535)$ two curves are presented: The dot-dashed line refers to the original set of input parameters with strong coupling (s) while the solid line refers to the new set with weaker coupling (w).

When the off-shell mass of a N^* resonance exceeds the ω -meson production threshold given by the ω pole mass ($m_N + m_\omega$), the decay width sharply increases since the narrow ω peak acts similar as a δ -function. The width of a resonance which lies below the ω pole and has already there a noticeable branching to this decay channel acquires a large width at the ω pole. Such a step-like behavior is not unusual. If there is a wide potential barrier of height U_0 ($= m_R + m_\omega$) the life time of a resonant state vanishes at an energy $E > U_0$ ($\mu > m_R + m_\omega$). Moreover, the life time can vanish sharply if the potential

barrier is flat (a square wall). Deeply below U_0 , the barrier penetration factor $D(E) = \exp(-2\sqrt{2m(U_0 - E)}a)$ is almost constant (with a being the barrier width), just below U_0 it increases exponentially, and just above U_0 $D(E) = 1$.

The $N^*(1535)$ off-shell partial width is especially large for the strong coupling amplitude (s), being 16 GeV above the ω threshold. We interpret this high $N^*(1535)$ width as an indication for a dissolving resonant state $N^*(1535)$ for running masses μ above the ω production threshold. Fig. 2 shows the spectral function of the $N^*(1535)$. One sees that when large values of the decay width appear (dashed curve), the resonance spectral function drops sharply above the ω production threshold which demonstrates from another side the disappearance of the resonant states with increasing running mass.

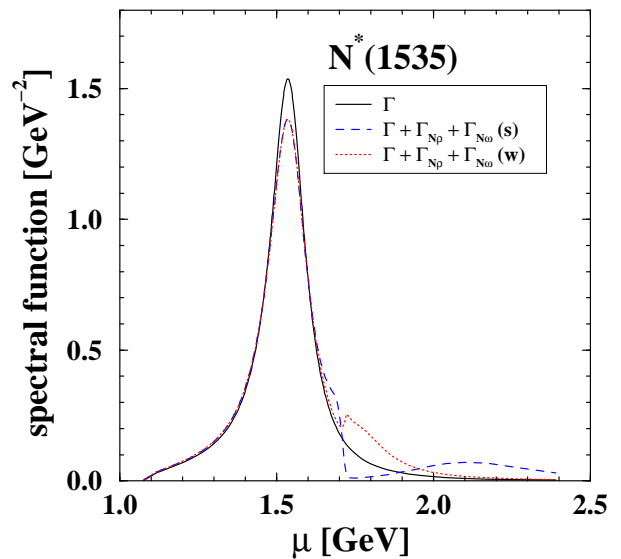


FIG. 2. Spectral distribution of the $N^*(1535)$ resonance using an energy dependent total width, and adding the partial $N\rho$ and $N\omega$ widths. The two cases of a strong (s) and weak (w) coupling to the $N\omega$ channel are distinguished.

The implication of a full dissolving of the $N^*(1535)$ is quite straightforward: Integrals over the running mass μ should be cutted at $\mu > m_R + m_\omega$. In our model, it comes out automatically through the appearance of the large total resonance width in the denominator of the Breit-Wigner distribution. The large width of $N^*(1535)$ demonstrates that we are somewhere above a potential barrier where the resonance does not exist any more. The resonance model still allows to treat all resonances on the same footing, accounting in the calculations of the cross section for the full energy range $m_p + m_\pi < \mu < \sqrt{s} - m_p$. In principle, the interval $m_p + m_\omega < \mu < \sqrt{s} - m_p$ does for the $N^*(1535)$ not significantly influence observables due to its suppression through the large $N^*(1535)$ width. It should, however, be mentioned that the scaling by the Blatt-Weisskopf factor leads to a drop of $\Gamma_{N\omega}^R$ at values

of μ larger than 2 GeV which results in the small bump which appears in the $N^*(1535)$ spectral function at high values of μ and gives some additional strength to the cross section at high energies. This fact has, however, no influence on the threshold behavior of the cross section on which the present work focuses.

The relatively large $N\omega$ resonance widths are not too surprising. The ω coupling to nucleons is 3 times greater than the ρ coupling, according to the $SU(3)$ symmetry. One can therefore expect that at equal kinematical conditions the off-shell $N\omega$ widths above the ω production threshold will typically be an order of magnitude greater than the $N\rho$ widths. The off-shell partial widths of the weakly coupled $N^*(1535)$ (solid curve) and of other resonances are below 1 GeV.

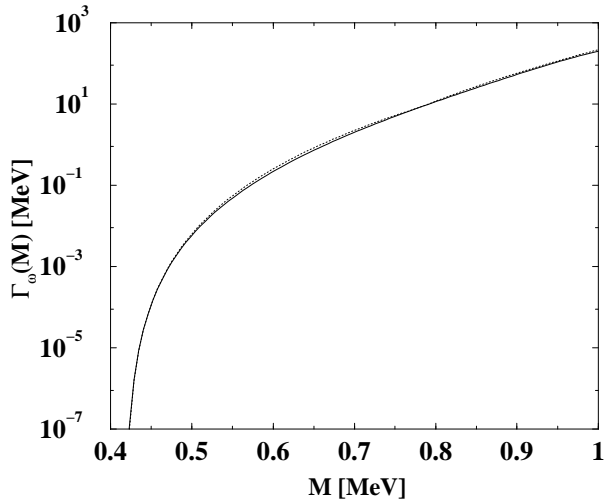


FIG. 3. The ω -meson decay width $\Gamma_\omega(M)$ versus the off-shell ω -meson mass M . The solid line shows the calculation (9) according to Gell-Mann, Sharp, and Wagner [31]. The dotted line is the parametrisation of Eq. (10).

Taking the spectral distribution of the ω meson into account the branching to the ω decay mode is given by

$$dB(\mu, M)^{R \rightarrow p\omega} = \frac{\Gamma_{N\omega}^R(\mu, M)}{\Gamma_R(\mu)} dW_\omega(M). \quad (8)$$

The energy dependence of the ω width $\Gamma_\omega(M)$ can be calculated according to the two-step process $\omega \rightarrow \rho\pi \rightarrow 3\pi$, as proposed by Gell-Mann, Sharp, and Wagner [31]. The effective vertices describing the $\omega \rightarrow \rho\pi$ and $\rho \rightarrow 2\pi$ decays have the form $\mathcal{L}_{\omega\rho\pi} = f_{\omega\rho\pi} \epsilon_{\tau\sigma\mu\nu} \partial_\sigma \omega_\tau \partial_\nu \rho_\mu^\alpha \pi^\alpha$ and $\mathcal{L}_{\rho\pi\pi} = -\frac{1}{2} f_{\rho\pi\pi} \epsilon_{\alpha\beta\gamma} \rho_\mu^\alpha \pi^\beta \partial_\mu \pi^\gamma$, with $f_{\omega\rho\pi} = 16.3 \text{ GeV}^{-1}$ and $f_{\rho\pi\pi} = 6.03$ (see e.g. [17]). The decay width can be found to be

$$\begin{aligned} \Gamma_\omega(M) = & \frac{1}{48\pi^5 M} f_{\omega\rho\pi}^2 f_{\rho\pi\pi}^2 \int_{4m_\pi^2}^{(M-m_\pi)^2} dM'^2 \int_{-1}^{+1} \frac{dz}{2} \\ & |D(k^+ + k^-) + D(k^+ + k) + D(k^- + k)|^2 \\ & \times (m_\pi^2 p^2 q^2 - p^2 (kq)^2 - q^2 (kp)^2) \\ & \times \Phi_2(M, M', m_\pi) \Phi_2(M', m_\pi, m_\pi) \end{aligned} \quad (9)$$

where m_π is the pion mass, k^+ , k^- , and k are the pion π^+ , π^- , and π^0 momenta, $p = k^+ + k^-$, $q = (k^+ - k^-)/2$, $p^2 = M'^2$, $kp = (M^2 - M'^2 - m_\pi^2)/2$, $q^2 = -p'^2(M', m_\pi, m_\pi)$, $kq = -p^*(M, M', m_\pi)p^*(M', m_\pi, m_\pi)Mz/M'$. The value of z is the cosine between the vectors \mathbf{q} and \mathbf{k} in the c.m. frame of the charged pions. $D(p)$ is the ρ -meson propagator with the total width of 150 MeV. The ω width is well interpolated by

$$\Gamma_\omega(M) = \Gamma_\omega(m_\omega) \left(\frac{p^*(M, m_\pi, 2m_\pi)}{p^*(m_\omega, m_\pi, 2m_\pi)} \right)^a \quad (10)$$

with the coefficient $a = 8$ at $M < m_\omega$ and $a = 10$ at $M > m_\omega$. The expression (10) is compared to Eq. (9) in Fig. 3. The ω width goes to zero at the $3m_\pi$ threshold which is also the physical ω threshold for the $pp \rightarrow pp\omega$ reaction.

The width (9) has still uncertainties away from the ω peak: First, the coupling constants $f_{\omega\rho\pi}$ and $f_{\rho\pi\pi}$ can be M -dependent. Also, the Blatt-Weisskopf factor which is not included here suppresses the off-shell widths above the resonance mass and enhances the off-shell widths below. It is applied usually to two-body decays. The ω decay has a three-body final state, so the appropriate modification of the spectral function is not straightforward. Notice that the $\omega \rightarrow 3\pi$ decay cannot simply be treated as a quasi two-body decay either, due to the coherent superposition of the ρ -meson propagators entering the integrand of Eq. (9). For the strong $N^*(1535)$ coupling, an enhancement at $M < m_\omega$ would result into a further increase of the off-shell part of the cross section as discussed below, but not into an increase of its peak measurable part. For the weak coupling, where the background is not very pronounced the cross section is practically not affected by this uncertainty.

III. THE $PP \rightarrow PP\omega$ CROSS SECTION

In this section we turn to the calculation of the ω production in pp reactions. We distinguish between the two scenarios of a strong, respectively a weak $N^*(1535)N\omega$ coupling. The decay modes of the other resonances are kept fixed as determined in [18] and given in Table 1.

A. Strong $N^*(1535) - N\omega$ coupling

First we consider the differential cross section $d\sigma/dM$. Fig. 4 shows the differential cross section $d\sigma/dM$ for typical excess energies of the SATURNE ($\epsilon = 3.8, 19.6, 30.1$ MeV) and the COSY-TOF ($\epsilon = 173$ MeV) experiments.

At small excess energies the cross section is dominated by off-shell omega production with masses far below the ω pole mass of 782 MeV. At the smallest considered energy of 3.8 MeV there is even no clear ω peak structure visible in the spectrum whereas at larger values of ϵ the ω peak is well developed. With increasing energy the

off-shell production with ω masses far below the quasi-particle pole becomes less important.

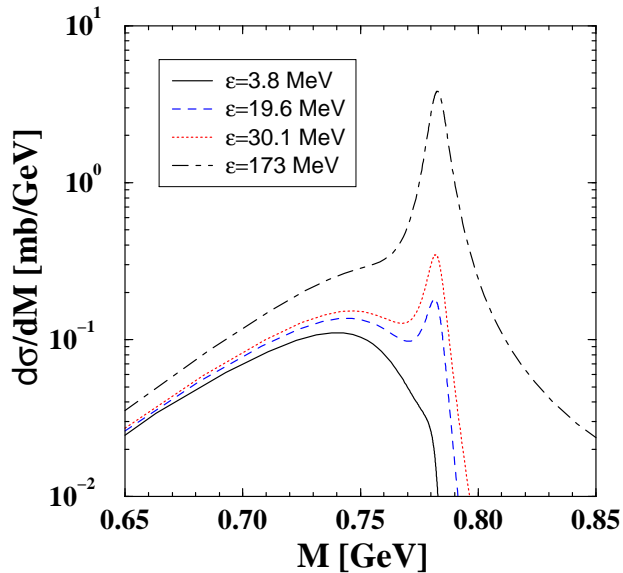


FIG. 4. Differential $pp \rightarrow pp\omega$ cross section as a function of the ω mass M calculated at different values of the excess energy ϵ .

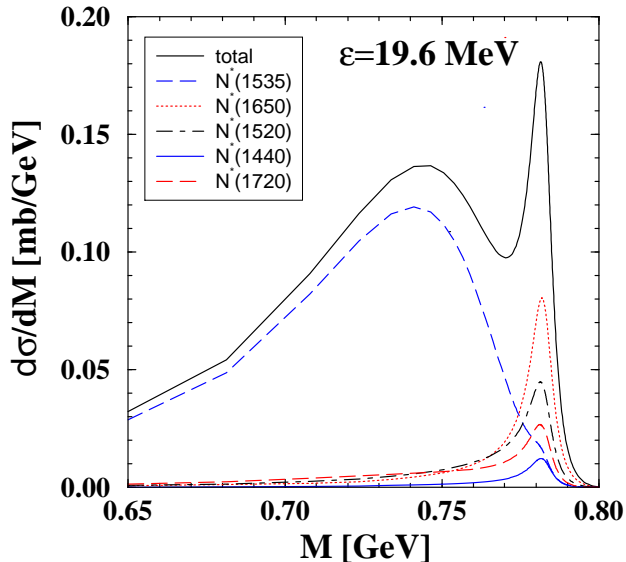


FIG. 5. Differential $pp \rightarrow pp\omega$ cross section as a function of the ω mass M calculated at an excess energy of $\epsilon = 19.6$ MeV. The contributions from the various resonances are shown separately.

E.g. at 173 MeV the off-shell strength is already moderate. Here the cross section originates to most extent from the ω peak but the off-shell part leads still to a non-vanishing renormalization of the cross section. Notice that suppression of the ω peak in the strong coupling

regime remains in force with increasing \sqrt{s} . While the integration region on Fig. 6 becomes larger, the effective integration region remains restricted by the ω pole mass. The relative contribution of the $N^*(1535)$ to the cross section therefore does not increase with the energy, as distinct from other resonances. It explains why the theoretical "background" becomes less important at high energy.

To explore the origin of the large off-shell component in more detail the next Fig. 5 shows separately the contributions of the various resonances at an excess energy of $\epsilon = 19.6$ MeV. As can be seen from there the decay of the $N^*(1535)$ is responsible for the large off-shell ω production with masses far below the pole mass whereas the off-shell contributions of the other resonances are small. However, at the ω pole the situation is opposite, i.e. the contribution from the $N^*(1535)$ is strongly suppressed whereas the other resonances show a clear peak structure.

The reason for this peculiar behavior of the $N^*(1535)$ lies in its large coupling to the $N\omega$ channel already far below the threshold (given by the physical ω mass). Since the decay width is large at the resonance pole which lies 167 MeV below the ω pole this resonance provides significant strength to the ω production in a kinematical regime where the ω meson is far off-shell. When the ω mass approaches the on-shell value the partial decay width to the $N\omega$ channel increases strongly. However, the strong increase suppresses the on-shell production of the meson. The suppression is already reflected in the spectral distribution of the $N^*(1535)$ resonance, shown in Fig. 2. This is a general feature for the decay of a broad resonance to another particle which arises under particular kinematical conditions. As discussed by Knoll for the case of the ρ decay [32] the opening of new decay channels suppresses generally the corresponding contributions at the on-shell values. The reason lies in the non-perturbative way by which the new channel enters into the resonance spectral function where it adds to the total resonance width [32]. In the case of the $N^*(1535)$ this effect is particularly pronounced due to the large $N\omega$ decay width and the corresponding kinematical conditions. At $\epsilon = 19.6$ MeV, the background generated by the $N^*(1535)$ remains below the experimental background [7]. It is also smooth enough to generate no visible structure in the data [7].

The mechanism which is responsible for the occurrence of the strong off-shell ω contribution is illustrated in Fig. 6. We show the kinematical limits for the integrations of the cross section, Eq. (1). The integration region is the two-dimensional parameter space of the off-shell ω -meson mass M and the off-shell N^* mass μ . We plot schematically along the horizontal axis the $N^* \rightarrow N\omega$ width as a function of μ . On the vertical axis, we show schematically the Breit-Wigner function for the ω -meson, which enters into Eq. (1). The sharp increase of the $N^* \rightarrow N\omega$ width can result in a strong suppression of the integrand in the shaded area, due to Breit-Wigner function (3). The ω peak appears just in the region where such a sup-

pression is possible. The occurrence of the "theoretical background" has therefore a simple kinematical origin. Whether it occurs depends on the off-shell $N^* \rightarrow N\omega$ width in the vicinity of the ω -meson production threshold. The integration boundaries for this example are determined for an excess energy of $\epsilon = 30$ MeV.

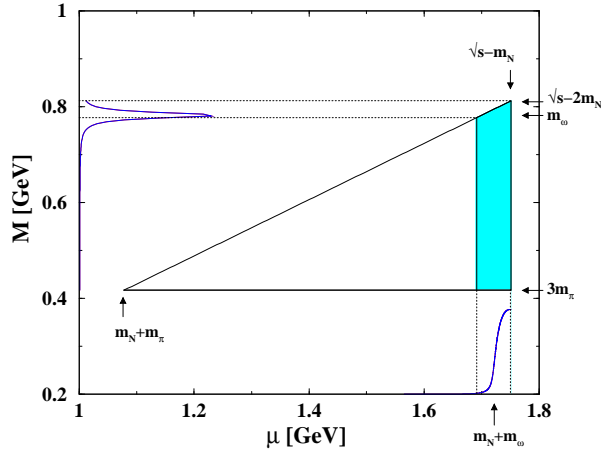


FIG. 6. The integration region for the ω production cross section is displayed. The integration is performed in the two-dimensional parameter space of the off-shell ω -meson mass M and the off-shell N^* mass μ . Along the horizontal axis the behavior of the $N^* \rightarrow N\omega$ width as a function of μ is indicated schematically, on the vertical axis the ω -meson spectral distribution is indicated. The sharp increase of the $N^* \rightarrow N\omega$ width can result in a strong suppression of the integrand in the dashed region where also the ω peak appears.

At small excess energies the cross section receives its major strength from off-shell ω production. However, experimentally only the ω peak can be identified in missing mass spectra and the off-shell part of the cross section is attributed to the general experimental background. Hence, for a meaningful comparison to data the same procedure has to be applied to theory which means to take only the contribution from the ω peak into account. The subtraction of this theoretical "background" due to off-shell meson production is demonstrated in Fig. 7 for $\epsilon = 19.6$ MeV. Like in the experimental analysis [8] the background is smoothly interpolated by splines. The remaining peak contribution resembles a Breit-Wigner distribution around the ω pole mass which, due to the energy dependence of Γ_ω and the phase space factor $\Phi_3(\sqrt{s}, m_p, m_p, M)$ entering into the cross section, is asymmetric. As soon as a clear peak structure is apparent, the decomposition of the cross section is straightforward and rather unique as indicated by the error bars shown in Fig. 8.

The correspondingly renormalized total cross section is shown in Fig. 8 as a function of the excess energy ϵ . It can be seen from there that the theoretical calculation provides now a very accurate description of the exclusive experimental ω cross section from close to threshold [7,8]

up to excess energies of several GeV. In particular, at low energies the slope of the cross section is well reproduced.

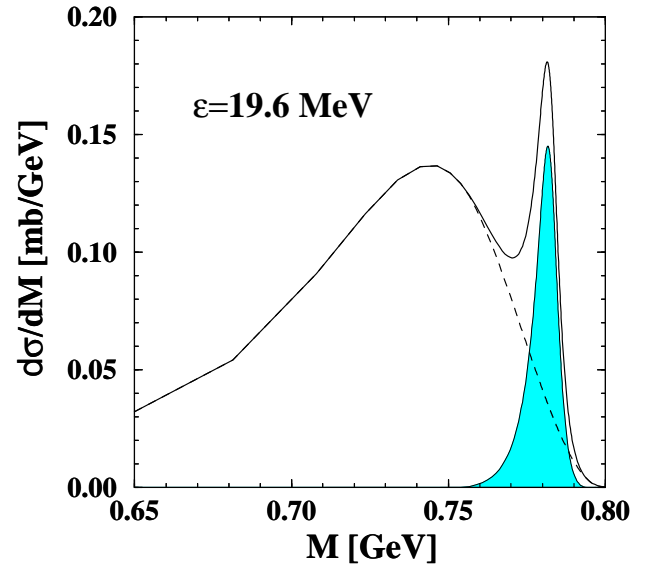


FIG. 7. Differential $pp \rightarrow pp\omega$ cross section at an excess energy of $\epsilon = 19.6$ MeV. The theoretical background due to off-shell ω production (dashed line) is subtracted from the full cross section (solid line). The hatched area shows the remaining contribution from the ω peak.

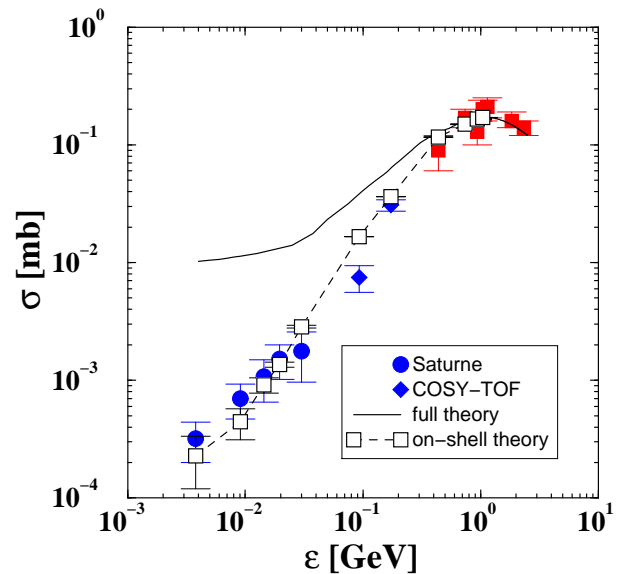


FIG. 8. Exclusive $pp \rightarrow pp\omega$ cross section obtained in the resonance model. Data are taken from [7,8] and [33,34]. The solid curve shows the full cross section including the contributions from off-shell ω production. The dashed curve corresponds to the renormalized cross section where only the experimentally detectable contribution from the ω peak is taken into account.

The full theoretical cross section, i.e. including also the off-shell ω production, is also shown in Fig. 8. The total cross section is systematically larger than the renormalized and the experimental cross sections. Above excess energies of the DISTO point [33] (440 MeV) the low energy off-shell production starts to become negligible and both curves almost coincide. Due to the increasing phase space of the ω width at large excess energies arise new off-shell contributions from the high momentum tail of the ω spectral function. Since the present work concentrates on the threshold behavior, we accounted only partially for high momentum corrections to the cross section which are small anyhow. However, close to threshold the contribution from the off-shell “background” to the total cross section is about one order of magnitude larger than the measurable pole part of the cross section.

B. Weak $N^*(1535) - N\omega$ coupling

If one assumes a coupling of the $N^*(1535)$ to the $N\omega$ channel which is 6 to 8 times weaker as in the previous case, according to the fit to the alternatively selected data set for this resonance (see the Appendix) the $pp \rightarrow pp\omega$ cross section has a completely different behavior close to threshold.

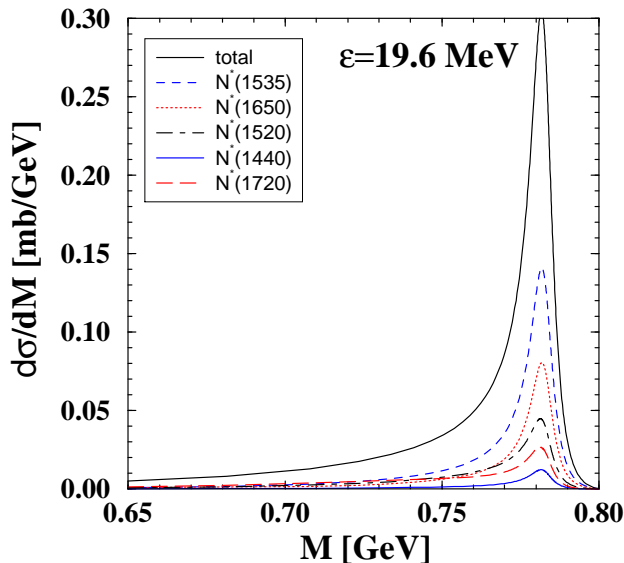


FIG. 9. Differential $pp \rightarrow pp\omega$ cross section as a function of the ω mass M calculated at an excess energy of $\epsilon = 19.6$ MeV. The contributions from the various resonances are shown separately.

We show the differential cross section again for $\epsilon = 19.6$ MeV. First of all, the large contribution from off-shell ω production vanishes. The remains still strength at masses far below the ω pole but compared to the previous case the off-shell production is almost negligible. On the other hand, the on-shell ω production from the $N^*(1535)$ is no

more suppressed but contributes now maximal to the on-shell cross section. Since the contributions from the other resonances remain unchanged the magnitude of the cross section at the ω pole mass is about 30 % larger as in the previous case. The deviation increases with decreasing \sqrt{s} .

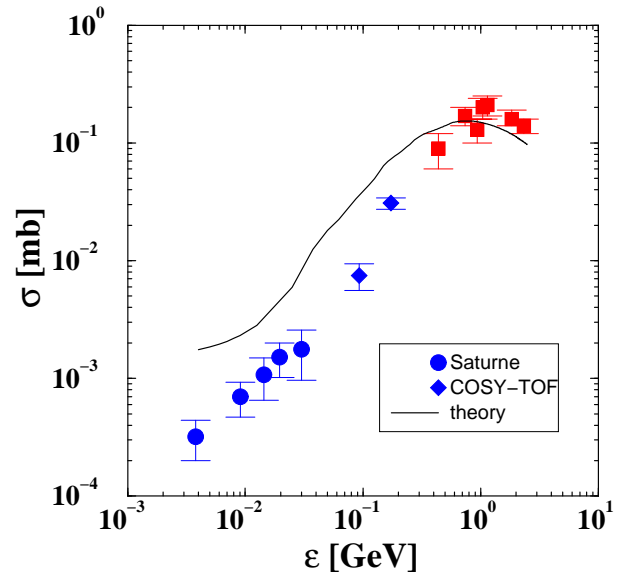


FIG. 10. Exclusive $pp \rightarrow pp\omega$ cross section obtained in the resonance model. Data are taken from [7,8] and [33,34].

Now the “theoretical background” due to off-shell production is much smaller than in the previous case and thus the distinction between the on-shell and the moderate off-shell part of the cross section is not straightforward. Nevertheless, very close to threshold the background is present and the cross section does not vanish when the excess energy ϵ goes to zero. When the ω meson is treated as an elementary field [12] the cross section, according to phase space, vanishes by construction at the threshold, however, here the physical threshold for the ω production is given by the $3m_\pi$ threshold instead of the ω pole mass. The threshold behavior is qualitatively similar to a recent calculation from Jülich group [35] where the finite mass distribution of the ω has been taken into account. However, close to threshold our result is significantly larger and overestimates the SATURNE [7] and COSY [8] data. A subtraction of the small and not so well defined off-shell background is now a delicate procedure which depends strongly on the particular experimental treatment of the background. We estimated the magnitude of this effect and found that it might bring the theoretical result into slightly better agreement with experiment at the lowest measured excess energies [7]. But already at $\epsilon = 30$ MeV and in particular for the COSY points [8] such corrections are practically zero and thus the experimental results are still overestimated. In the COSY regime the tendency is similar as in the calculations from [12,35] which also overestimate the data due

to a too strong rise of the theoretical cross sections with energy.

At large excess energies above 1 GeV the cross section is somewhat reduced compared to the case with large $N^*(1535) - N\omega$ coupling and also compared to experiment. The reason is missing strength from this resonance at high energies. This behavior is already reflected in the spectral function, Fig. 2. The large $N^*(1535) - N\omega$ coupling depletes the spectral function at the ω threshold and shifts strength to the high energy tail which is missing in the second case. There the strength is concentrated around and above (a few hundred MeV) the ω threshold which results in the enhanced cross section in the COSY regime.

In ref. [11], the experimental results were compared to a cross section which is assumed to be proportional to the $NN\omega$ phase space corrected by the proton-proton S-wave final state interaction and the finite ω width. It was pointed out that the energy of the protons is sufficiently high to get higher partial waves where the proton-proton correlations are not important and that a smooth interpolation of the cross section to lower \sqrt{s} is valid provided that there are no nucleon resonances strongly coupled to the $N\omega$ channel. Apparently, our model is based on the opposite assumption that all the dynamics is governed by the nucleon resonances. We reproduce all the data above $\epsilon = 500$ MeV well, but our interpolation to the lower energies is different from [11]. With respect to the FSI, our model is complementary in the sense that we take into account the $N\omega$ final state interactions by including nucleon resonances, whereas the proton-proton FSI is missing. Near the threshold, the proton-proton FSI enhances the amplitude which is relevant for the SATURNE data [7]. For the weak $N^*(1535)$ coupling, the amplitude in our model is overestimated already due to the inclusion of the $N\omega$ FSI. Adding a $NN\omega$ contact term with strongly correlated S-wave nucleons, the description of the data would require an amplitude of opposite sign and a delicate cancellation between the proton-proton and the $N\omega$ FSI at threshold. The resonance model proposed by Teis et al. [19] has a contact term for a direct $NN\pi$ coupling which could be attributed to the NN FSI. Its contribution is, however, not so important at threshold for the $pp\pi$ final states. On the other side, taking solely the resonance contributions into account underestimates the $pn\pi^0$ cross section at threshold. This fact can be interpreted to mean that the proton-proton FSI is effectively included to the phenomenological matrix elements for the production of nucleon resonances. Concerning the strong $N^*(1535)$ coupling, the data are nicely reproduced without proton-proton FSI, which is probably less important than the considered $N\omega$ FSI.

In summary, the comparison to the data favors the calculation based on the large $N^*(1535)N\omega$ branching ratio. An additional fact which supports this picture is the strongly anisotropic $pp\omega$ angular distribution observed in [8] at $\epsilon = 173$ MeV. As can be seen from Table 1 only the $N^*(1535)$ has a large s -wave compo-

nent in the $N\omega$ decay. The contributions from the other resonances involve higher partial waves which lead to anisotropic angular distributions. As we have seen, the strong $N^*(1535)N\omega$ coupling suppresses the contribution from this resonance at the ω pole which leads to the following decomposition of the on-shell cross section at $M = m_\omega$: $N^*(1535)$ (7%), $N^*(1650)$ (26%), $N^*(1520)$ (17%), $N^*(1440)$ (22%) and $N^*(1720)$ (26%). Hence the on-shell cross section contains only a small s -wave component. In the alternative case the s -wave contribution from the $N^*(1535)$ is much larger, the cross section decomposes according to: $N^*(1535)$ (35%), $N^*(1650)$ (18%), $N^*(1520)$ (12%), $N^*(1440)$ (15%) and $N^*(1720)$ (18%). An highly anisotropic angular distribution indicates furthermore that contribution from meson exchange currents which are missing in our treatment are small [12].

IV. SUMMARY

The ω production in nucleon-nucleon collisions has been described via the excitation of nucleon resonances. The approach is based on the extended VMD (eVMD) model which successfully describes the mesonic $R \rightarrow NV$ and radiative $R \rightarrow N\gamma$ decays of nucleon resonances. Among the considered resonances the $N^*(1535)$ turns out to play a special role for the ω production. The reason is a large decay mode to the $N\omega$ channel in a kinematical regime where the ω is far off-shell. A strong $N^*(1535)N\omega$ coupling is implied by the available electro- and photo-production data. As a consequence large off-shell contributions in the ω production cross section appear. In particular close to threshold the off-shell production is dominant. On the other hand, the on-shell production of ω mesons at their physical masses is suppressed, since above the ω production threshold the $N^*(1535)$ acquires a large width and dissolves. This feature appears generally when a broad resonance has a large branching to a narrow state already far below the pole mass of the produced particle. In quantum mechanics, a similar behavior is experienced by resonance states at energies just above a potential barrier.

We found that near threshold, the off-shell production of the ω 's becomes dominant. This part of the cross section can, however, be hardly identified experimentally and is attributed currently to the background. To compare to data we applied the same procedure as experimentalists: The theoretical "background" from the off-shell production was subtracted and only the measurable pole part of the cross section was taken into account. Doing so, the available data are accurately reproduced starting from energies very close to threshold up to energies significantly above threshold without adjusting any new parameters. At small excess energies the full cross section is about one order of magnitude larger than the measurable pole part.

Since the observed results depend crucially on the role of the $N^*(1535)$ we considered also an alternative scenario which is possible within experimental uncertainties. Since the $N\omega$ decay of this resonance has not been measured directly, the existing $N\rho$ data leave some freedom to fix the eVMD model parameters. A different normalization to the $N\rho$ channel, making thereby use of an alternative set of quark model predictions, allows to reduce the $N\omega$ decay mode by maximally a factor of 6 to 8, however, on the price of a slightly worse reproduction of the existing data set. With the reduced $N\omega$ coupling the $N^*(1535)$ shows no extraordinary behavior and the off-shell contributions are substantially reduced. However, this resonance contributes now fully to the peak part of the cross section which leads to a significant overestimation of the experimental data around and several 100 MeV above threshold.

We conclude that, consistent with the analysis of electro- and photoproduction data, the measured ω production in pp reactions favors the scenario of a large coupling of the $N^*(1535)$ to the $N\omega$ channel. The consequences are large off-shell contributions in the ω production cross section around threshold. Experimentally this part of the cross section is hardly accessible since it is hidden in the general experimental background. However, if the off-shell ω production is large, the number of dileptons produced in pp collisions should be significantly greater than one would expect from estimates based on the on-shell production of ω 's. This effect should manifest itself in the description of the dilepton production in pp collisions at kinetic beam energies which correspond to the ω -meson threshold. It can have consequences for the dilepton production in heavy-ion collisions.

The hypothesis of a large off-shell ω production is also appealing from another point of view. The ϕ meson decays dominantly to the $K\bar{K}$ mode with a threshold very close to the physical ϕ mass. Hence one does not expect sizable off-shell effects in this case. When off-shell ω 's are counted, the ϕ/ω ratio could come into agreement with the OZI rule, i.e. the experimentally observed deviations from the OZI predictions for the ϕ/ω ratio might be explained by the neglect of the off-shell ω -meson production.

Acknowledgments

The work was supported by GSI (Darmstadt) under the contract TÜFÄST, by the Plesler Foundation, and by the Deutsche Forschungsgemeinschaft under contract No. 436RUS113/367/0(R).

- [1] R. Machleidt, *Adv. Nucl. Phys.* **19**, 189 (1989).
- [2] G.E. Brown and M. Rho, *Phys. Rev. Lett.* **66**, 2720 (1991); *ibid.*, *Phys. Rep.* **269**, 333 (1996).
- [3] T. Hatsuda and S.H. Lee, *Phys. Rev.* **C46**, R34 (1992); Y. Koike, *Phys. Rev.* **C51**, 1488 (1995); T. Hatsuda, S.H. Lee, H. Shiomi, *Phys. Rev.* **C52**, 3364 (1992); S. Leupold, *Phys. Rev.* **C64**, 015202 (2001).
- [4] F. Klingl, N. Kaiser, W. Weise, *Nucl. Phys.* **A624**, 527 (1997); M. Urban, M. Buballa, R. Rapp, J. Wambach, *Nucl. Phys.* **A641**, 433 (1998); *ibid.*, **A673**, 357 (2000); R. Rapp, J. Wambach, *Adv. Nucl. Phys.* **25**, 1 (2000); W. Peters, M. Post, H. Lenske, S. Leupold, and U. Mosel, *Nucl. Phys.* **A632**, 109 (1998).
- [5] B. Friman, H.J. Pirner, *Nucl. Phys.* **A 617**, 496 (1997).
- [6] G. Agakichiev et al. [CERES Coll.], *Phys. Rev. Lett.* **75**, 1272 (1995); M. Masera [HELIOS-Coll.], *Nucl. Phys.* **A590**, 93c (1995); W.K. Wilson et al. [DLS Coll.], *Phys. Rev.* **C57**, 1865 (1998); J. Friese [HADES Coll.], *Nucl. Phys.* **A654**, 1017c (1999).
- [7] F. Hibou et al., *Phys. Rev. Lett.* **83**, 492 (1999).
- [8] S. Abd El-Samad et al. [COSY-TOF Coll.], *Phys. Lett.* **B522**, 16 (2001).
- [9] S. Okubo, *Phys. Lett.* **B5**, 165 (1965); G. Zweig, CERN Report No 8419/Th 412; I. Iizuka, *Prog. Theor. Phys. Suppl.* **37-38**, 21 (1966).
- [10] H.J. Lipkin, *Phys. Lett.* **B60**, 371 (1976); J. Ellis, *Phys. Lett.* **B353**, 319 (1995).
- [11] F. Balestra *et al.* [DISTO Coll.], *Phys. Rev. Lett.* **81**, 4572 (1998).
- [12] K. Nakayama, A. Szczurek, C. Hanhart, J. Haidenbauer, J. Speth, *Phys. Rev.* **C57**, 1580 (1998).
- [13] D. M. Manley and E. M. Saleski, *Phys. Rev. D* **45**, 4002 (1992).
- [14] T. P. Vrana, S. A. Dytman and T. S. Lee, *Phys. Rept.* **328**, 181 (2000).
- [15] R. Koniuk, *Nucl. Phys. B* **195**, 452 (1982).
- [16] M. Lutz, Gy. Wolf, B. Friman, *Nucl. Phys.* **A706**, 431 (2002).
- [17] M. Post, U. Mosel, *Nucl. Phys.* **A688**, 808 (2001).
- [18] M. I. Krivoruchenko, B. V. Martemyanov, A. Faessler and C. Fuchs, *Annals Phys. (N.Y.)* **296**, 299 (2002).
- [19] S. Teis, W. Cassing, M. Effenberger, A. Hombach, U. Mosel, and Gy. Wolf, *Z. Phys.* **A356**, 421 (1997).
- [20] A. Faessler, C. Fuchs, M. I. Krivoruchenko and B. V. Martemyanov, *nucl-th/0010056*.
- [21] V. A. Matveev, R. M. Muradian and A. N. Tavkhelidze, *Lett. Nuovo Cim.* **7**, 719 (1973); S. J. Brodsky and G. R. Farrar, *Phys. Rev. Lett.* **31**, 1153 (1973); *Phys. Rev. D* **11**, 1309 (1975); A. I. Vainstein and V. I. Zakharov, *Phys. Lett. B* **72**, 368 (1978).
- [22] G. Hohler, E. Pietarinen, I. Sabba Stefanescu, F. Borkowski, G. G. Simon, V. H. Walther and R. D. Wendling, *Nucl. Phys. B* **114**, 505 (1976).
- [23] M. I. Krivoruchenko and A. Faessler, *Phys. Rev. D* **65**,

017502 (2002).

- [24] A. Faessler, C. Fuchs and M. I. Krivoruchenko, Phys. Rev. C **61**, 035206 (2000).
 [25] R.J. Porter et al. [DLS Coll.], Phys. Rev. Lett. **79**, 1229 (1997).
 [26] Particle Data Group, Phys. Rev. **D54** (1996).
 [27] R. Koniuk, Nucl. Phys. B **195**, 452 (1982).
 [28] D. M. Manley and E. M. Saleski, Phys. Rev. D **45**, 4002 (1992).
 [29] S. Capstick and W. Roberts, Phys. Rev. D **49**, 4570 (1994).
 [30] D. E. Groom *et al.* [Particle Data Group Coll.], Eur. Phys. J. C **15** (2000) 1.
 [31] M. Gell-Mann, D. Sharp, G.W. Wagner, Phys. Rev. Lett **8**, 261 (1962).
 [32] J. Knoll, Prog. Part. Nucl. Phys. **42**,177 (1999).
 [33] F. Balestra et al. [DISTO Coll.], Phys. Rev. **C63**, 024004 (2001).
 [34] V. Flaminio et al., CERN-HERA 84-10 (1984).
 [35] K. Nakayama, J.W. Durso, J. Haidenbauer, C. Hanhart, J. Speth, Phys. Rev. **C60**, 055209 (1999).

V. APPENDIX

Fig. 11 shows two different fits to the electro- and photoproduction data, the πN multichannel scattering, and the quark model predictions for the $N^*(1535)$ resonance. The difference between the two procedure lies in the normalizations to the ρ -meson decay amplitudes. The original fit of [18] (dot-dashed lines) is based on the results of refs. [27,28,30]. The quark model of Koniuk [27], the πN analysis of Manley and Saleski [28], and the PDG [30] give close predictions for the $s_{1/2}$ wave and predict the same sign for the $d_{3/2}$ wave. Using this set of data the solution is rather stable and yields a large $N\omega$ $s_{1/2}$ wave amplitude.

The second set of amplitudes (solid lines) stems from the based on the quark model calculations by Capstick and Roberts [29]. Their values are noticeable smaller than those proposed by [27,28,30]. It allows the reduction of the amplitude by a factor of 6 to 8, however, by the price of a moderately higher χ^2 . A further going reduction of the amplitude is hardly possible. The deviation from the experiment for the Coulomb amplitude of the $p^*(1535)$ becomes then stronger and the quality of the fit for the transversal amplitude of the $p^*(1535)$ is also worse, but the ρ -meson amplitudes are reproduced better than for the first set of input parameters. Notice that the $d_{3/2}$ amplitude of the ω -meson was set equal to zero to ensure an unique eVMD solution to the fitted data.

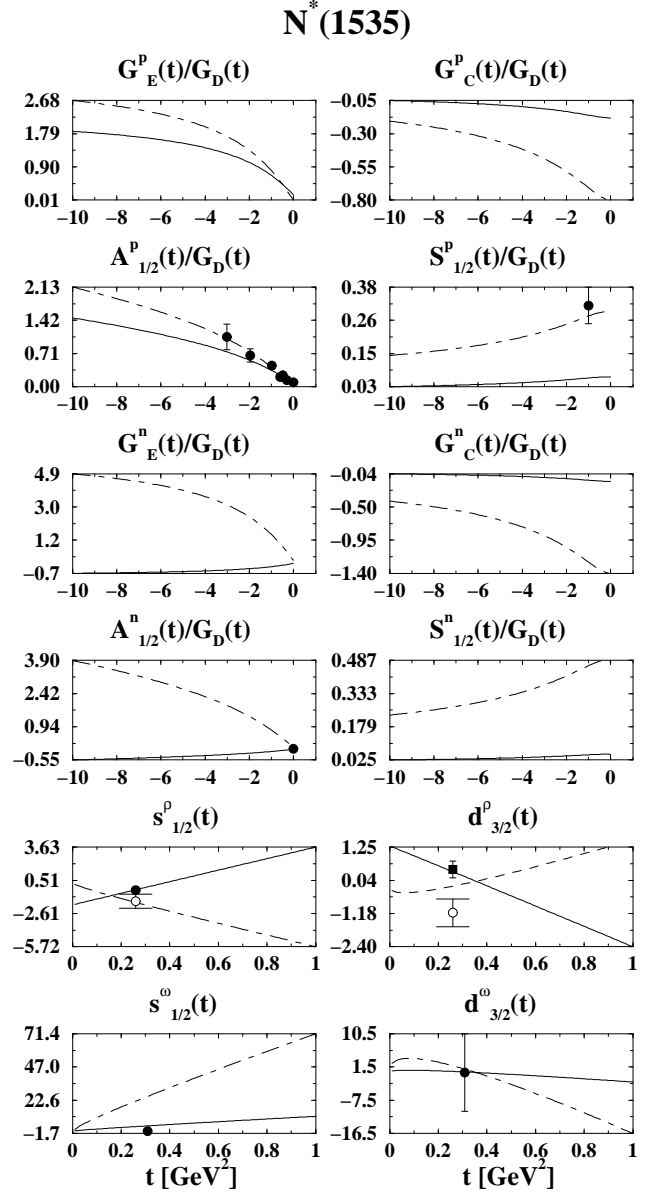


FIG. 11. Electromagnetic transition form factors of the magnetic, electric, and Coulomb types (G_M , G_E , and G_C), helicity amplitudes ($A_{3/2}$, $A_{1/2}$, and $S_{1/2}$), and partial-wave amplitudes of nucleon resonance decays into the ρ - and ω -meson channels for the $N^*(1535)$ resonance. The value $G_D(t) = 1/(1-t/0.71)^2$ is the dipole function. The photo- and electro-production experimental data [30] are displayed. The ρ meson decay amplitudes (filled symbols) are from [30,28,27], the opaque circles are the quark model predictions from [29]. The dot-dashed lines correspond to fit to the strong coupling set [30,28,27], while the solid lines correspond to the weak coupling set [29].

□

TABLE I. Resonances (R) included into the $NN \rightarrow NN\omega$ cross section through the two-step mechanism $NN \rightarrow NR$, $R \rightarrow N\omega$. The second column shows the total widths of the resonances. The third column shows the partial widths for $N\omega$ decays ($\sqrt{\Gamma_{N\omega}}$ in $\text{MeV}^{1/2}$). The next three columns show the partial-wave decomposition of the $N\omega$ widths, including signs of the amplitudes. The coupling constants g_M , g_E , and g_C at the ω pole are given in the last three columns in units GeV^{-l+1} ($J = l + 1/2$). The $N\omega$ decay modes are determined by fitting the photo- and electro-production data, results of the multichannel πN partial-wave analysis, and quark model predictions [18]. In the case of the $N^*(1535)$, the results from the two different fits with a strong (s), respectively, and a weak (w) $N\omega$ branching are given.

Resonance	Γ_0 [MeV]		$\sqrt{\Gamma_{N\omega}}$ [$\text{MeV}^{1/2}$]	$N\omega$	$N\omega$	$N\omega$	g_M	g_E	g_C
$N^*(1535)\frac{1}{2}^-$	150	s:	1.43	$s_{1/2}$	$d_{3/2}$				
		w:	0.21	1.43	0.05			-28.03	-42.67
$N^*(1650)\frac{1}{2}^-$	150		0.21	0.21	0.01			-4.22	-6.34
$N^*(1650)\frac{1}{2}^-$	150		0.97	-0.97	-0.02			2.01	4.14
$N^*(1520)\frac{3}{2}^-$	120		0.29	$d_{1/2}$	$d_{3/2}$	$s_{3/2}$	-7.67	18.16	46.13
$N^*(1520)\frac{3}{2}^-$	120		0.29	-0.02	0.03	0.28			
$N^*(1675)\frac{5}{2}^-$	150		0.06	$d_{1/2}$	$d_{3/2}$	$g_{3/2}$	2.07	-1.61	-10.50
$N^*(1675)\frac{5}{2}^-$	150		0.06	0.06	< 0.01	< 0.01			
$N^*(1440)\frac{1}{2}^+$	350		< 0.01	$p_{1/2}$	$p_{3/2}$		-14.14		63.13
$N^*(1440)\frac{1}{2}^+$	350		< 0.01	< 0.01	< 0.01				
$N^*(1720)\frac{3}{2}^+$	150		5.69	$p_{1/2}$	$p_{3/2}$	$f_{3/2}$	0.14	-8.27	-37.73
$N^*(1720)\frac{3}{2}^+$	150		5.69	5.29	-2.09	0.14			
$N^*(1680)\frac{5}{2}^+$	130		0.71	$f_{1/2}$	$f_{3/2}$	$p_{3/2}$	-1.34	-11.75	-7.98
$N^*(1680)\frac{5}{2}^+$	130		0.71	0.09	0.58	0.40			